Journal of Alloys and Compounds 509 (2011) 1217–1221

Contents lists available at ScienceDirect

Journal of Alloys and Compounds

journal homepage: www.elsevier.com/locate/jallcom

# Monodisperse water-soluble Fe–Ni nanoparticles for magnetic resonance imaging

Hong Yang, Xuejian Li, Hong Zhou, Yeming Zhuang, He Hu, Huixia Wu, Shiping Yang*

*Department of Chemistry, Shanghai Normal University, 100 Guilin Road, Shanghai 200234 PR China*

ARTICLE INFO

*Article history:*
Received 20 July 2010
Received in revised form
28 September 2010
Accepted 29 September 2010
Available online 8 October 2010

*Keywords:*
MRI
Fe–Ni nanoparticles
Transverse relaxivity
Cytotoxicity

ABSTRACT

Monodispersed Fe–Ni nanoparticles (NPs) with the diameter around 9 nm were synthesized by high temperature pyrolysis of iron(III) acetylacetonate and nickel(II) acetylacetonate. Ligand exchange method with a bifunctional bisphosphonate was adopted to improve the water solubility. To prevent their biofouling and aggregate in the biological system, the prepared NPs were further covalent conjugated with the PEG acid. Their morphology and structure were confirmed by TEM, XRD and FTIR. NPs showed good magnetic properties with the saturation magnetization (Ms) of about 40 emu/g and the transverse relaxivity ($r_2$) of about 43.1 $mM^{-1}$ $s^{-1}$ in aqueous solutions. Furthermore, Fe–Ni NPs showed low cytotoxicity in living cells. They can be uptaken by HeLa cells effectively and result in the obvious effect of $T_2$-weighted MRI of labeled cells after internalization, making them potential contrast agents for MRI study.



## 1. Introduction

Magnetic resonance imaging (MRI) is currently one of the most powerful *in vivo* imaging technologies due to its noninvasive property and multidimensional tomographic capabilities coupled with high spatial resolution [1–4]. To obtain the high contrast and information-rich images for disease detection, contrast agents (CAs) play a prominent role in magnetic resonance imaging. The current MRI contrast agents are in the form of $T_1$-positive agents of paramagnetic species and $T_2$-negative agents of superparamagnetic nanoparticles (NPs). Generally, complex-based CAs have a relatively short residence time in the vascular system and display toxicity due to the existence of free metal ions, which limits their clinical applications [5]. Therefore, superparamagnetic NPs are extremely popular and they have shown outstanding results in the field of imaging *in vitro* and *in vivo* [6–13]. Transition metal alloy NPs are considered to be of great potential for their application because of their relatively high saturation magnetizations ($M_s$) except conventional superparamagnetic iron oxide (e.g., $Fe_2O_3$ and $Fe_3O_4$) and ferrite NPs [14].

Recently, Dai and co-workers reported FeCo NPs stabilized with single graphitic carbon shells for integrated diagnosis and therapeutic (photothermalablation) applications [15]. Maenosono et al. prepared water-soluble superparamagnetic FePt NPs with a mean diameter of 9 nm and indicated that they might be superior negative CAs for magnetic resonance imaging [16]. Recently, our group developed monodispersed amphiphilic FePt NPs *via* a one-step pyrolysis reaction in the presence of tetraethylene glycol and oleic acid that could serve as an effective MR cell-labelling agent [17]. To the best of our knowledge, there have been a few reports about the application of water-soluble Fe–Ni NPs as MRI contrast agents [18].

In this work, we developed a high temperature thermal decomposition approach to synthesize oleylamine-capped Fe–Ni NPs (Fe–Ni@OA NPs). They can only be dispersed in nonpolar organic solvents because of the long alkyl chain of the capping molecules. But for biomedical applications, it is indispensable to transfer these NPs to an aqueous phase. Therefore, to transform Fe–Ni@OA NPs into the hydrophilic NPs, ligand exchange method was adopted with a bifunctional bisphosphonate ligand [(4-amino-1-hydroxy-1-phosphono-butyl)-phosphonic acid sodium salt, abbreviated as APAS in the text]. Bisphosphonates cannot only stabilize inorganic core efficiently due to the strong fixation moiety and but also have an interesting biological activity [19–21]. To prevent the biofouling of nanoparticles in blood plasma and formation of aggregates that are quickly sequestered by cells of the reticular endothelial system (RES) such as macrophages, the NPs were further covalent conjugated with the PEG acid reacted by reaction with primary amine units on the surface of Fe–Ni@APAS NPs (Scheme 1).

## 2. Experimental

### 2.1. Reagents and characterization

Iron chloride, nickel chloride, acetylacetone and triethylamine were purchased form Sinopharm Chemical Reagent Co., Ltd. Oleylamine was purchased from J&K

* Corresponding author.
*E-mail address:* shipingy@shnu.edu.cn (S. Yang).

0925-8388/$ – see front matter © 2010 Elsevier B.V. All rights reserved.
doi:10.1016/j.jallcom.2010.09.191

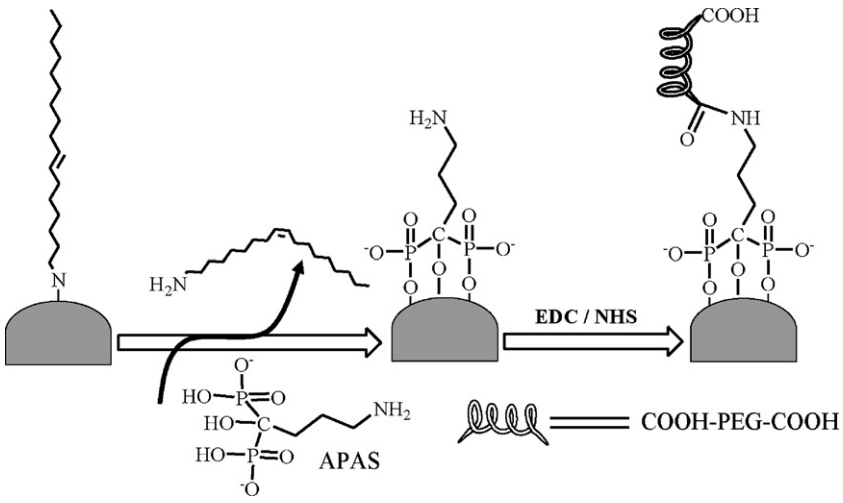


**Scheme 1.** Surface modification process of Fe–Ni@APAS@PEG NPs.

Chemical Reagent Co., Ltd. PEG diacid (Mw: 600) was purchased form Aldrich Chemicals Inc.

X-ray diffraction (XRD) measurements were determined by a Rigaku DMAX 2000 diffractometer equipped with Cu/Kα radiation at a scanning rate of 4°/min in the $2\theta$ range from 20 to 80°($\lambda$ = 0.15405 nm) (40 kV, 40 mA). Transmission electron microscope (TEM), high-resolution TEM (HRTEM) images were obtained on a JEOL JEM 2010 electron microscope at an accelerating voltage of 200 KV. Samples for TEM analysis were prepared by spreading a drop of as-prepared products dilute dispersion on amorphous carbon-coated copper grids and then dried in air. Fourier transform infrared (FT-IR) spectra were recorded on a Perkin-Elmer Spectrum one spectrometer. Hysteresis loop was measured with a vibrating sample magnetometer VSM-236 (LAKE SHORE, America). The metal ions concentrations were quantified using inductively coupled plasma atomic emission spectroscopy (ICP-AES) (Perkin-Elmer Optima 5300 DV). The $T_1$-weighted images were acquired with a conventional spin echo acquisition (TR 3500 ms) with TE values of 1000 μs, section thickness of 0.6 mm. $T_1$ relaxivities were measured in a 0.5 T magnet (Shanghai Niumag Corporation ration NM120-Analyst) at room temperature. Relaxivity values of $r_1$ were calculated through the curve fitting of $1/T_1$ relaxation time ($s^{-1}$) *vs.* the Fe concentration (mM). The $T_2$-weighted images were acquired with a conventional spin echo acquisition (TR 1000 ms) with TE values of 6000 μs, section thickness of 0.6 mm. $T_2$ relaxivities were performed in a 0.5 T magnet (Shanghai Niumag Corporation ration NM120-Analyst) at room temperature. Relaxivity values of $r_2$ were calculated through the curve fitting of $1/T_2$ relaxation time ($s^{-1}$) *vs.* the Fe concentration (mM).

### 2.2. Preparation of Fe–Ni@OA NPs

$Ni(acac)_2$ and $Fe(acac)_3$ were synthesized according to the literature [22].

In a typical synthesis procedure, 2.25 mmol of $Ni(acac)_2$, 0.75 mmol $Fe(acac)_3$, and 21 mL of oleylamine were added into a reaction flask and the mixture was heated to 130 °C and kept at this temperature for 20 min, and then fast heated to 300 °C and maintained for 30 min before cooling down to room temperature. After centrifugation at 10,000 rpm for 15 min, the supernatant was removed and a black precipitate was obtained. The resulting black precipitate was washed with ethanol for several times to acquire Fe–Ni@OA NPs. Fe–Ni@OA NPs can be easily re-dispersed in various organic solvents such as hexane, toluene, and dichloromethane. Finally, they were dried in vacuum before use.

### 2.3. Preparation of Fe–Ni@APAS NPs

4 mL (15 mg/mL) of the Fe–Ni@OA NPs ethanol solution was mixed with APAS (1.1 g, 0.34 mmol), 2 ml tetramethylammonium hydroxide pentahydrate (TMAH) and 20 mL of water. The mixture was then stirred vigorously for 12 h at room temperature, and the solution was centrifuged with distilled water for five times, and Fe–Ni@APAS NPs were obtained.

### 2.4. Preparation of Fe–Ni@APAS@PEG NPs

The PEG diacid (300 mg, 0.5 mmol) were activated with 1-ethyl-3-(3-dimethyl aminopropyl) carbodimide (EDC) (96 mg, 0.5 mmol) and N-hydroxysuccinimide (NHS, 143 mg, 1.25 mmol) in 40 mL DMSO solution for 2 h. Subsequently Fe–Ni@APAS NPs (10 mL, 8 mM) in DMSO were added to the above solution and stirred vigorously for 7 h at room temperature. The reaction mixture was centrifuged and washed with distilled water for many times to remove excess the PEG diacid. Then Fe–Ni@APAS@PEG NPs were obtained.

### 2.5. Cytotoxicity assay

A human cervical carcinoma cell line (HeLa cells) were provided by Shanghai Institutes for Biological Sciences (SIBS), Chinese Academy of Sciences (CAS, China). Cells were cultured in DMEM (Dulbecco's Modified Eagle Medium) supplemented with 10% FBS at 37 °C and 5% $CO_2$. Cells were plated in tissue culture flask under the 100% humidity.

*In-vitro* cytotoxicity was evaluated by performing methyl thiazolyl tetrazolium (MTT) assays on the HeLa cells. Cells were seeded into a 96-well cell culture plate at $2 \times 10^5$/well in DMEM with 10% FBS at 37 °C and 5% $CO_2$ for 24 h, then the cells were incubated with Fe–Ni@APAS@PEG NPs with different concentrations (0, 5, 10, 20, 40, 60, 100 μg/mL diluted in DMEM) for 12 h at 37 °C under 5% $CO_2$. Thereafter, MTT (10 μL, 5 mg/mL) was added to each well and the plate was incubated for 4 h at 37 °C. The assays were carried out according to the manufacturer's instructions. The OD 490 value (Abs.) of each well was measured by Thermo Multiskan MK3-based microplate reader.

## 3. Results and discussion

Fe–Ni@OA NPs were prepared by the high temperature pyrolysis method *via* the precursors of $Ni(acac)_2$ and $Fe(acac)_3$ in oleylamine under an inert atmosphere according to the method reported by Peng et al. [23] The crystallography of the products was verified by powder X-ray diffraction (XRD) (Fig. 1a). And all the diffraction peaks of the as-prepared Fe–Ni NPs can be clearly indexed as an awaruite Fe–Ni (JCPDS card No.: 38-0419) phase. The broadening of the diffraction peaks distinctly indicates the nanocrystalline

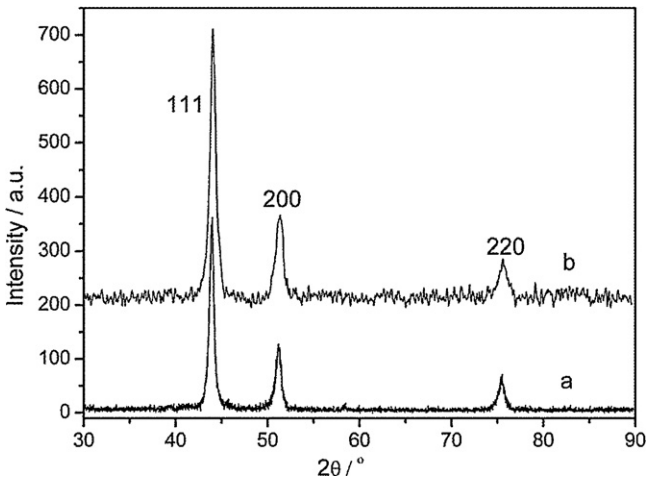


**Fig. 1.** X-ray diffraction pattern of Fe–Ni@OA NPs (a) and Fe–Ni@APAS@PEG NPs (b).

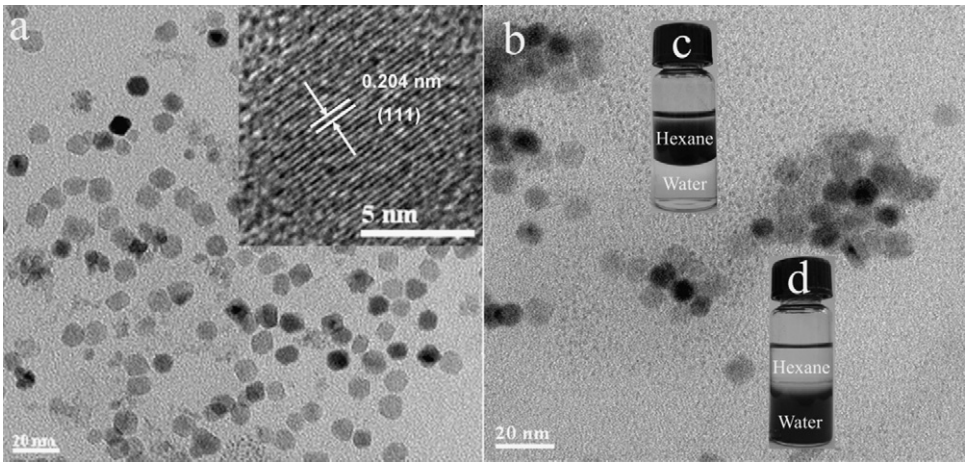


**Fig. 2.** TEM micrograph of Fe–Ni@OA NPs (a) and Fe–Ni@APAS@PEG NPs (b). Inset in a: high resolution TEM image of Fe–Ni@OA NPs. Inset in b: the visual photograph of Fe–Ni@OA NPs (c) and Fe–Ni@APAS@PEG NPs in hexane/water mixture solvent (d).

nature of the materials. Fe–Ni@OA NPs was monodispersed and had a spherical shape with a diameter around 9 nm (Fig. 2a). High resolution TEM image (Fig. 2a inset) of the particles reveals the high crystalline nature of Fe–Ni@OA NPs. The lattice spacing between two adjacent planes is 0.204 nm, which corresponds to the d spacing for the (1 1 1) lattice plane very well. The stoichiometry of Fe–Ni was determined to be 2.2 by dissolving the metal species in a mixed acid solution, and measuring the Fe and Ni concentrations on the basis of ICP.

Fe–Ni@OA NPs are only soluble in hexane and other nonpolar or weakly polar organic solvents such as chloroform (Fig. 2c). For biological application, water solubility of NPs is indispensable. By the ligand exchange method, a bisphosphonate ligand (ASPS) was firstly used to replace the original surfactant OA on the surface of Fe–Ni NPs via strong coordination interaction to give Fe–Ni@APAS NPs. At this stage, the surface of NPs is functionalized with amine groups facilitating the hydrophobic Fe–Ni NPs' dispersing in aqueous media or further functionalization [6,24]. To prevent their biofouling and aggregate in the biological system, the PEG was covalently anchored on the surface of the particles with one of the carboxylic groups in the PEG diacid *via* the EDC/NHS coupling reaction. After coating, NPs were able to disperse in water to form a clear solution (See Fig. 2d). The XRD pattern (Fig. 1b) confirmed the crystallography of NPs did not changed yet after surface modification. From the TEM images, no obvious difference for the core size of NPs was observed after surface coating as shown in Fig. 2b. The Fe–Ni@APAS@PEG NPs had a narrow size distribution with an average hydrodynamic size of 269 nm further checked using dynamic light scattering analysis.

The surface of Fe–Ni@APAS@PEG NPs was further characterized by Fourier-transform infrared (FTIR) spectroscopy (Fig. 3). Fe–Ni@OA NPs showed some main absorption peaks in IR spectrum. Two broad bands at 3450 and 1635 $cm^{-1}$ can be ascribed to the N–H stretching vibration and $NH_2$ stretching, and another around 2900 $cm^{-1}$ is referenced to the stretching vibration of C–H. All FTIR characterizations prove that the presence of oleylamine on the Fe–Ni NPs surface. After the ligand exchange, the P–O stretching absorption arises between 1200 and 800 $cm^{-1}$. After functionalized with PEG acid, Fe–Ni@APAS@PEG NPs exhibit a broad peak at ~1100 $cm^{-1}$, which is due to the characteristic stretching vibration of C–O–C group of PEG.

The magnetic property of Fe–Ni@OA NPs, Fe–Ni@APAS NPs and Fe–Ni@APAS@PEG NPs was evaluated on a vibrating sample magnetometer with an applied field of $-5\,kOe < H < 5\,kOe$ at room temperature. The hysteresis loop of the samples shown in Fig. 4

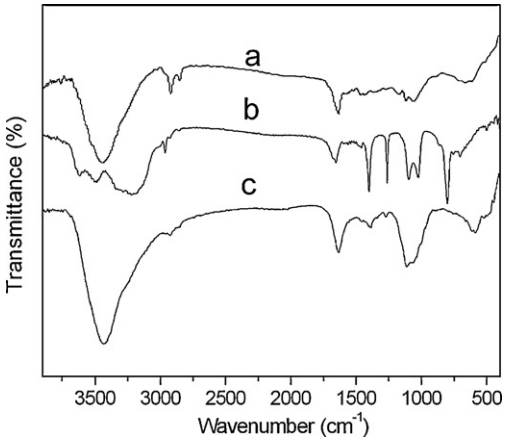


**Fig. 3.** FTIR spectra of Fe–Ni@OA NPs (a), Fe–Ni@APAS NPs (b) and Fe–Ni@APAS@PEG NPs (c).

revealed that they are ferromagnetic at room temperature. The saturation magnetization (Ms), remanent magnetization (Mr), and coercivity (Hc) values for the NPs are shown in Table 1.

To further investigate the contrast effect, the specific relaxivities ($r_1$ or $r_2$) were measured of Fe–Ni@APAS@PEG NPs. The transverse relaxation ($T_2$) and longitudinal relaxation time ($T_1$) of

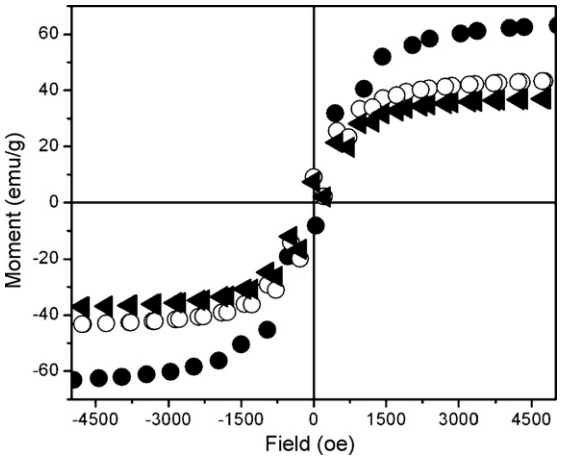


**Fig. 4.** The room-temperature hysteresis loop of Fe–Ni@OA (●), Fe–Ni@APAS (○) and Fe–Ni@APAS@PEG (◄).

**Table 1**
Magnetic Data of Obtained Fe–Ni NPs at room temperature.

| Fe–Ni NPs | Ms (emu/g) | Mr (emu/g) | Mr/Ms | Hc (Oe) |
|---|---|---|---|---|
| Fe–Ni@OA | 63.0 | 9.6 | 0.15 | 203.7 |
| Fe–Ni@APAS | 42.6 | 7.8 | 0.18 | 177.3 |
| Fe–Ni@APAS@PEG | 36.9 | 5.9 | 0.16 | 172.3 |

Fe–Ni@APAS@PEG NPs were measured at 0.5 T in order to investigate the MR signal effects. The MR assays of $T_1$ and $T_2$-weighted imaging show the imaging enhancement at various Fe ion concentrations of Fe–Ni@APAS@PEG NPs (Fig. 5a). The $T_2$-weighted MR signals of Fe–Ni@APAS@PEG NPs decreased at Fe ion concentrations of 0.427 mM, indicating that Fe–Ni@APAS@PEG NPs could be used as a $T_2$ MR imaging contrast agent. In the $T_1$-weighted imaging sequences for Fe–Ni@APAS@PEG NPs, the MR imaging intensity substantially become bright with increasing iron ion concentrations up to a high concentration of 1.715 mM, showing a weak $T_1$ effect. The $T$ relaxation rate ($1/T_{1,2}$) as a function of the Fe concentration for Fe–Ni@APAS@PEG NPs (Fig. 5b) show that the relaxation rate increases linearly with the Fe concentration according to the following equation:

$$\frac{1}{T_{1,2}} = \frac{1}{T^0_{1,2}} + r_{1,2}[\mathrm{Fe}]$$

Where $1/T_{1,2}$ is the observed relaxation rate in the presence of Fe–Ni@APAS@PEG NPs, $1/T^0_{1,2}$ the relaxation rate of pure water, [Fe] the concentration of Fe–Ni@APAS@PEG NPs, and $r_{1,2}$ the transverse and longitudinal relaxivity. The $r_1$ and $r_2$ value of Fe–Ni@APAS@PEG NPs was calculated to be 0.7 and 43.1 $mM^{-1}\ s^{-1}$, respectively. The Fe–Ni@APAS@PEG NPs had a high $r_2/r_1$ value (61.6), suggesting a potential use as a negative MRI contrast agent [25].

Generally, the cytotoxicity of nanoparticles is critical to the biomedical application. Fig. 6 showed the cell viability results for HeLa cells incubated with different concentration Fe–Ni@APAS@PEG NPs for 12 h by the MTT assay. No significant decrease in the proliferation of the HeLa cells could be observed with the studied concentration range of Fe–Ni@APAS@PEG NPs.

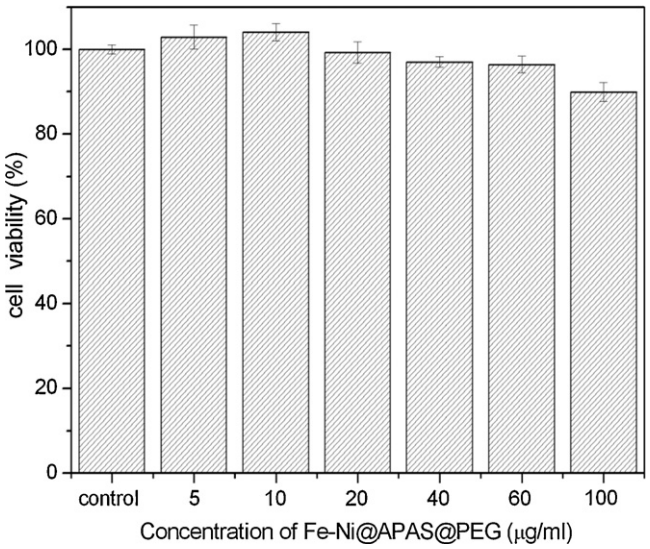


**Fig. 6.** Cytotoxicity profile of Fe–Ni@APAS@PEG NPs *via* MTT assay on HeLa cells.

Thus, the Fe–Ni@APAS@PEG NPs showed good biocompatibility and little toxicity against the model cell lines, and it would be a potential MRI contrast agent *in vitro* and *vivo*.

To validate the potential of the Fe–Ni@APAS@PEG NPs as an MRI cell tracking probe, the $T_2$-weighted imaging of the HeLa cells after incubation for 7 h with the Fe–Ni@APAS@PEG particles at different sample concentrations are shown in Fig. 7a. The resulting $T_2$-weighted MR images of the cells incubated with Fe–Ni@APAS@PEG NPs at 0.5 T presented the clear contrast when comparing with that of the control cells without treatment. Comparable results were obtained by the quantitative analysis of the cellular iron and nickel contents by ICP-MS (Fig. 7b). After 7 h the cellular iron contents after incubation at 10 μg/mL, 40 μg/mL, 80 μg/mL and 100 μg/mL were 1.73, 3.94, 7.21 and 10.3 pg/cell, respectively. These results clearly show that Fe–Ni@APAS@PEG NPs can be uptaken by cells in

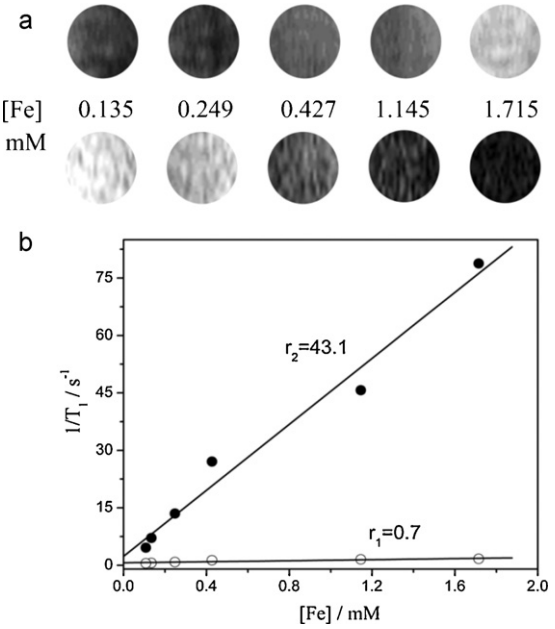


**Fig. 5.** (a) $T_1$-weighted MR images (upper part of Panel a) and $T_2$-weighted MR images (lower part of Panel a) of Fe–Ni@APAS@PEG NPs in water containing 0.5% xanthan gum. (b) $T_1$ and $T_2$ relaxivity plot of aqueous suspension of Fe–Ni@APAS@PEG NPs.

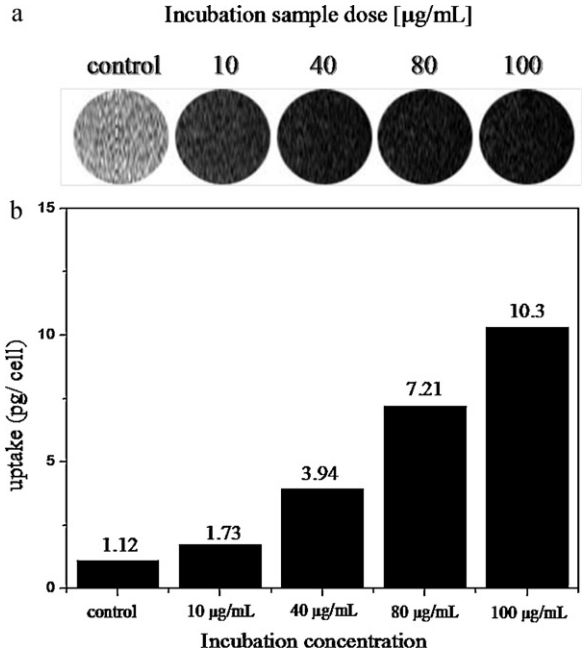


**Fig. 7.** (a) $T_2$-weighted MR images of containing unlabeled control cells and Fe–Ni@APAS@PEG NPs-labeled cells at different incubated sample concentrations for 7 h. (b) Iron uptake content in HeLa cells treated at different incubation concentrations for 7 h.

a concentrations-dependent manner for further MRI applications in biological systems.

## 4. Conclusions

In summary, superparamagnetic Fe–Ni NPs were synthesized by high temperature pyrolysis. By use of the ligand exchange method, water soluble NPs were obtained. The as-prepared Fe–Ni NPs showed high saturation magnetization (Ms) of about 40 emu/g and the transverse relaxivity ($r_2$) of about 43.1 $mM^{-1}$ $s^{-1}$ in aqueous solutions. The cytotoxicity results showed that Fe–Ni NPs were of low cytotoxicity in living HeLa cells. They are intensely internalized into HeLa cells. Therefore, they can be used as a new nanoparticulate MRI contrast agent.

## Acknowledgments

This work was financially supported by the National Natural Science Foundation of China, (50802059, 20971086), Shanghai Municipal Education Commission (09YZ159, 10ZZ84), the Shanghai Science and Technology Development Fund (09QA1404300) and the Excellent Youth Teachers of Shanghai University (RE902).

## References

[1] J. Cheon, J.H. Lee, Acc. Chem. Res. 41 (2008) 1630–1640.
[2] A.H. Lu, E.L. Salabas, F. Schuth, Angew. Chem. Int. Ed. 46 (2007) 1222–1244.
[3] Y.W. Jun, J.W. Seo, A. Cheon, Acc. Chem. Res. 41 (2008) 179–189.
[4] L.M. De Leon-Rodriguez, A.J.M. Lubag, C.R. Malloy, G.V. Martinez, R.J. Gillies, A.D. Sherry, Acc. Chem. Res. 42 (2009) 948–957.
[5] K.N. Raymond, V.C. Pierre, Bioconjugate Chem. 16 (2004) 3–8.
[6] H. Yang, Y. Zhuang, H. Hu, X. Du, C. Zhang, X. Shi, H. Wu, S. Yang, Adv. Func. Mater. 20 (2010) 1733–1741.
[7] C. Wilhelm, F. Gazeau, Biomaterials 29 (2008) 3161–3174.
[8] B. Chertok, B.A. Moffat, A.E. David, F.Q. Yu, C. Bergemann, B.D. Ross, V.C. Yang, Biomaterials 29 (2008) 487–496.
[9] N. Nasongkla, E. Bey, J.M. Ren, H. Ai, C. Khemtong, J.S. Guthi, S.F. Chin, A.D. Sherry, D.A. Boothman, J.M. Gao, Nano Lett. 6 (2006) 2427–2430.
[10] I.J.M. de Vries, W.J. Lesterhuis, J.O. Barentsz, P. Verdijk, J.H. van Krieken, O.C. Boerman, W.J.G. Oyen, J.J. Bonenkamp, J.B. Boezeman, G.J. Adema, J.W.M. Bulte, T.W.J. Scheenen, C.J.A. Punt, A. Heerschap, C.G. Figdor, Nat. Biotechnol. 23 (2005) 1407–1413.
[11] G. Lv, F. He, X.M. Wang, F. Gao, G. Zhang, T. Wang, H. Jiang, C.H. Wu, D.D. Guo, X.M. Li, B.A. Chen, Z.Z. Gu, Langmuir 24 (2008) 2151–2156.
[12] Z. Shi, K.G. Neoh, E.T. Kang, B. Shuter, S.-C. Wang, C. Poh, W. Wang, ACS Appl. Mater. Interfaces 1 (2009) 328–335.
[13] B. Feng, R.Y. Hong, Y.J. Wu, G.H. Liu, L.H. Zhong, Y. Zheng, J.M. Ding, D.G. Wei, J. Alloys Compd. 473 (2009) 356–362.
[14] H. Yang, C. Zhang, X. Shi, H. Hu, X. Du, Y. Fang, Y. Ma, H. Wu, S. Yang, Biomaterials 31 (2010) 3667–3673.
[15] W.S. Seo, J.H. Lee, X.M. Sun, Y. Suzuki, D. Mann, Z. Liu, M. Terashima, P.C. Yang, M.V. McConnell, D.G. Nishimura, H.J. Dai, Nat. Mater. 5 (2006) 971–976.
[16] S. Maenosono, T. Suzuki, S. Saita, J. Magn. Magn. Mater. 320 (2008) L79–L83.
[17] H. Yang, J. Zhang, Q. Tian, H. Hu, Y. Fang, H. Wu, S. Yang, J. Magn. Magn. Mater. 322 (2010) 973–977.
[18] M.-F. Tai, J.-K. Hsiao, S.-C. lee, S.-T. Chen, Chin. J. Process Eng. 6 (2006) 249–252.
[19] D. Portet, B. Denizot, E. Rump, J.-J. Lejeune, P. Jallet, J. Colloid Interface Sci. 238 (2001) 37–42.
[20] Y. Lalatonne, C. Paris, J.M. Serfaty, P. Weinmann, M. Lecouvey, L. Motte, Chem. Commun. (2008) 2553–2555.
[21] G. Baldi, D. Bonacchi, M.C. Franchini, D. Gentili, G. Lorenzi, A. Ricci, C. Ravagli, Langmuir 23 (2007) 4026–4028.
[22] H.W. Gu, R.K. Zheng, X.X. Zhang, B. Xu, J. Am. Chem. Soc. 126 (2004) 5664–5665.
[23] Y. Chen, X. Luo, G.-H. Yue, X. Luo, D.-L. Peng, Mater. Chem. Phys. 113 (2009) 412–416.
[24] J. Xie, S. Peng, N. Brower, N. Pourmand, X.W. Shan, S. Sun, Pure Appl. Chem. 78 (2006) 1003–1004.
[25] N. Hyon Bin, S. In Chan, H. Taeghwan, Adv. Mater. 21 (2009) 2133–2148.